Available online at www.eccomasproceedia.org
Eccomas Proceedia SMART (2025) 128-138

ECCOMAS
Proceedia

XI ECCOMAS Thematic Conference on Smart Structures and Materials - SMART 2025
M. Krommer, M. Nader and M. Schagerl (Eds)

Received: 28 April 2025 / Revised: 24 June 2025 / Accepted: 3 October 2025

Adaptive Resonant Piezoelectric Shunt Using Tunable Inductance

Arthur Haudeville, Adrien Queste, Christophe Giraud-Audine, Boris Lossouarn, Xavier Amandolese, Olivier Thomas

Abstract. Resonant piezoelectric shunts are highly effective for reducing vibrations of a structural natural mode. However, they require a fine tuning on the mechanical resonance to ensure that performances are optimal. This paper proposes a novel adaptive resonant piezoelectric shunt circuit and investigates its ability to adjust the value of the inductance. This circuit is thus used to vary the electrical frequency of the shunt and it proposes a robust strategy for vibration mitigation of a linear resonance. The principle involves incorporating a static converter controlled by a pulse-width modulation (PWM) circuit between the piezoelectric patch and the inductance. PWM is performed thanks to four-quadrant switches. It is demonstrated that the resonance frequency is linearly governed by the duty cycle of the PWM, with a range extending from zero hertz to the resonance frequency of the initial circuit. After numerical validation of the proposed circuit, a preliminary experimental validation is performed on a simple resonant LC circuit. It is observed that the resonance is indeed modified as expected. Some practical limitation yet appears, mainly due to the inductance internal resistance.

Key words: Resonant piezoelectric shunts, Adaptive shunt, Tunable inductance, Pulse-width modulation, Vibration mitigation

Arthur Haudeville & Adrien Queste & Christophe Giraud-Audine
Laboratoire d'Electrotechnique et d'Electronique de Puissance (L2EP), Univ. Lille, Arts et Metiers, Institute of Technology, Centrale Lille, Junia, ULR 2697, 8 Bd Louis XIV, 59000 Lille, France,
e-mail: christophe.giraud-audine@ensam.eu

Arthur Haudeville & Boris Lossouarn & Xavier Amandolese
Laboratoire de Mecanique des Structures et des Systemes Couples (LMSSC), Conservatoire national des arts et metiers (Cnam), 292 Rue Saint-Martin, 75000 Paris, France,
e-mail: boris.lossouarn@lecnam.net

Olivier Thomas
Laboratoire d'Ingenierie des Systemes Physiques et Numeriques (LISPEN), Ecole nationale superieure des arts et metiers (Ensam), 8 Bd Louis XIV, 59000 Lille, France,
e-mail: olivier.thomas@ensam.eu

ISSN:3078-543X. Published by Eccomas Proceedia.
Peer-review under responsibility of the organizing committee of SMART 2025.
doi: 10.7712/150125.13621.201007

1 INTRODUCTION

This work is part of the HYDRAVIB project where the aim is to perform hydrofoils' vibrations mitigation thanks to resonant piezoelectric shunts. Indeed, hydrofoils under a hydrodynamic flow are subjected to flow-induced vibrations [1], causing noise disturbances and structural fatigue. Resonant piezoelectric shunt circuits have been proven effective in mitigating vibrations of submerged hydrofoils [2, 3]. A typical passive resonant piezoelectric shunt consists of an electrical inductance L and resistance R connected in series, inducing an antiresonance effect on the mechanical response. However, optimal vibration suppression at a structural natural frequency demands precise tuning of both the resistance and inductance parameters [4]. Yet, in case of a structure under a hydrodynamic flow where a complex fluid-structure coupling operates, fixing values of R and L may resulting in weak performances of the shunt regarding the vibration mitigation. In marine applications, structures vibrating in hydrodynamic flows are prone to excitation across multiple natural frequencies due to time-varying flow velocities. Conventional approaches require a separate shunt circuit for each target natural frequency [5], a constraint that has motivated the development of adaptive shunt systems. Such systems aim to enhance robustness in complex dynamical systems and eliminate the need for multiple shunted circuits to suppress vibrations in case of sweeping excitation over multiple natural frequencies.

Adaptive shunt solutions, including electromagnetic [6, 7] or piezoelectric [8, 9] configurations, have been explored to emulate tunable electrical characteristics through active electronics. An alternative approach leverages standard PWM-based chopper circuits to achieve tunable resonant shunts. Demonstrated for electromagnetic systems [10], this method utilizes high-frequency switching to enable precise power modulation while avoiding complex active components. In this paper, this principle is adapted to modify the characteristics of the resonant RL piezoelectric shunt. Choppers of the electrical circuit modify the inductance value and so the electrical resonance frequency. The proof of concept is detailed in the next section with a simplified resonant electrical circuit. In a second step, the concept is extended to the model of a piezoelectric shunt coupled to the structure in the case of linear resonance. At last, an experimental validation of the PWM electronic circuits on a RLC circuit is performed.

2 PRINCIPLE OF A TUNABLE RESONANT CIRCUIT USING PWM

2.1 Average equivalent circuit

The operating principle of the adaptive shunt circuit is illustrated in Fig. 1. For simplicity, the piezoelectric patch is represented by an equivalent electrical circuit comprising a voltage source E in series with a capacitor C_P. Components L (inductance) and R (resistance) define the adaptive shunt, while R_L denotes the parasitic resistance of the inductance. The switches are assumed ideal (their practical implementation is addressed later) and are driven in a complementary manner, to achieve pulse-width modulation (PWM). During each switching period T_{PWM}, switch **A** conducts for a duration $\beta\, T_{\text{PWM}}$ (duty cycle β), connecting the piezoelectric patch to the inductance. For the remaining period, switch **B** conducts, disconnecting the patch and short-circuiting the inductance to interrupt power exchange between the components.

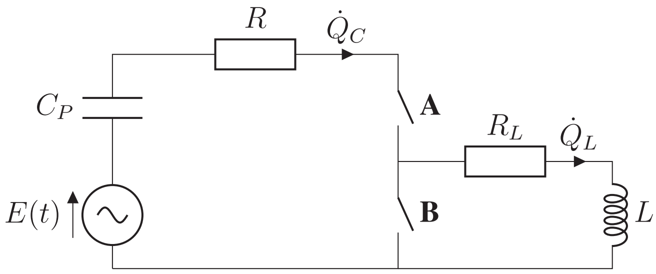

Figure 1: Simplified RLC circuit with tunable inductance thanks to the chopper with pulse-width modulation of the two switches.

Regarding the first configuration of the PWM, with the switch **A** closed and the switch **B** open, the electrical circuit is a classical RLC one with components in series and the Kirchhoff's law yields to

$$\begin{cases} L\dot{I}_L + (R + R_L)I_L + \dfrac{1}{C_P}Q_C = E\,, \\ \dot{Q}_C = I_L\,, \end{cases} \tag{1}$$

where Q_C is the electric charge in the capacitor and I_L is the current through the inductance. When the PWM operates in its second state (switch **A** open, switch **B** closed), a decaying current persists in the inductance branch (L). Kirchhoff's voltage law yields

$$\begin{cases} L\dot{I}_L + R_L I_L = 0\,, \\ \dot{Q}_C = 0\,. \end{cases} \tag{2}$$

Introducing the state vector $x = [I_L\ Q_C]^T$, Eq. (1, 2) can be written in the state-space form as $\dot{x}(t) = A_i\, x(t) + b_i\, u(t)$, for $i = \{1, 2\}$, with $u = \{E\}_2^T$ the driving function and

$$A_1 = \begin{pmatrix} \frac{-(R+R_L)}{L} & \frac{-1}{LC_P} \\ 1 & 0 \end{pmatrix}, \; b_1 = \begin{pmatrix} \frac{1}{L} \\ 0 \end{pmatrix} \quad \text{and} \quad A_2 = \begin{pmatrix} \frac{-R_L}{L} & 0 \\ 0 & 0 \end{pmatrix}, \; b_2 = \begin{pmatrix} 0 \\ 0 \end{pmatrix}. \tag{3}$$

Considering the PWM pulsation much larger than the electrical pulsation of the circuit $\omega_{\text{PWM}} \gg \omega_e = 1/\sqrt{LC_P}$, it has been shown in [10] that the average state-space system can be written as

$$\dot{x}(t) \simeq \bar{A}\, x(t) + \bar{b}\, u(t) \quad \text{with} \quad \begin{cases} \bar{A} = \beta A_1 + (1-\beta)A_2\,, \\ \bar{b} = \beta b_1 + (1-\beta)b_2\,. \end{cases} \tag{4}$$

Then, the average dynamical equation of the RLC electrical circuit of Fig. 1 can be given as an equivalent resonant circuit as in the following expressions:

$$\frac{L}{\beta^2}\ddot{Q}_C + \frac{\beta R + R_L}{\beta^2}\dot{Q}_C + \frac{1}{C_P}Q_C = E\,, \tag{5}$$

where one can infer the equivalent electrical pulsation $\bar{\omega}_e$ and the electrical damping ζ_e:

$$\bar{\omega}_e = \frac{\beta}{\sqrt{LC_P}} = \beta\omega_e \ , \qquad \bar{\zeta}_e = \frac{R + R_L/\beta}{2}\sqrt{\frac{C_P}{L}} \ . \tag{6}$$

The PWM adjusts the electrical resonance of the circuit proportionally to the duty cycle β by modifying the effective value of the inductance L/β^2. Moreover, it appears that the PWM also impacts the electrical damping $\bar{\zeta}_e$ and so the resonance magnitude.

2.2 Tunable resonant electrical circuit

Thanks to Eq. (5), the Fourier transform of $E(t)$ is operated and the electrical admittance of the resonant circuit $\dot{Q}_C/E$ is given by

$$Y(\Omega) = \frac{j\,\Omega\,\breve{Q}_C}{\breve{E}} = \frac{j\,\Omega\,\bar{\omega}_e^2\,C_P}{\bar{\omega}_e^2 - \Omega^2 + 2j\bar{\zeta}_e\Omega\bar{\omega}_e} \ , \tag{7}$$

where j stand for the imaginary number and $\breve{\circ}(\Omega)$ denotes the Fourier transform of $\circ(t)$. Note that the resonance occurs at $\Omega = \bar{\omega}_e$ and one can deduce from Eq. (7) the theoretical maximal electrical admittance $Y_{\text{max}} = \beta^2/(\beta R + R_L)$.

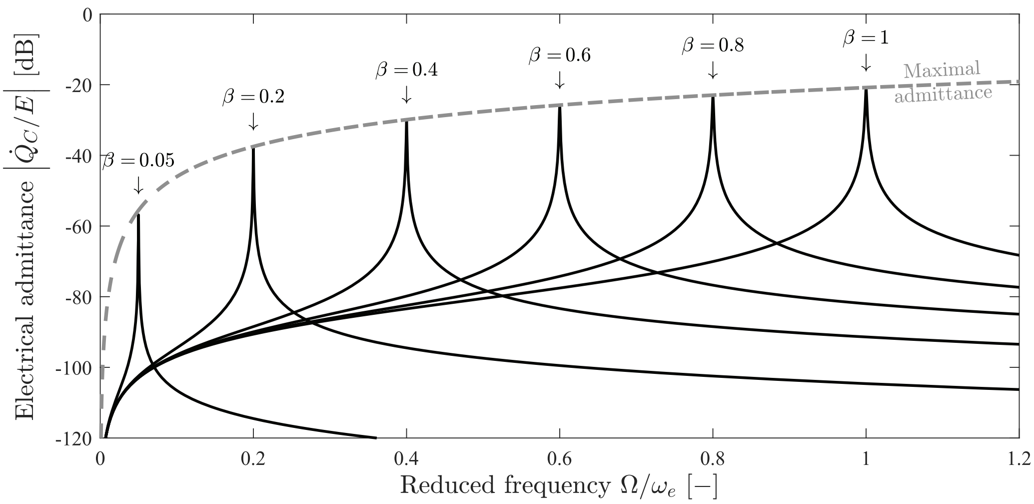

Figure 2: Modulus of the theoretical electrical admittance of Eq. (7), represented in solid lines (——), with $C_P = 40\,\text{nF}$, $R = 10\,\Omega$, $R_L = 1\,\Omega$, $L = 2\,\text{H}$ and a set of values β; The maximal admittance Y_{max}, represented in dashed lines (- - -), is calculated by defining the duty cycle as $\beta = \Omega/\omega_e$.

Fig. 2 confirms the linear dependence of the electrical resonance frequency on the duty cycle β. Furthermore, the operating range spans the full normalized frequency spectrum ($\Omega \in [0,\ \omega_e]$, corresponding to $\beta \in [0,\ 1]$).

3 THEORY OF THE TUNABLE PIEZOELECTRIC SHUNT

3.1 Governing equations

The model of the electrical circuit is extended to include the vibrational dynamics of the underlying structure coupled through a piezoelectric patch. The mechanical displacement w of the structure is expended on the $N \in \mathbb{N}^*$ natural mode basis of the structure,

$$w(t) = \sum_{j=1}^{N} \Phi_j \, q_j(t) \; , \tag{8}$$

where Φ_j and $q_j(t)$ are the j-th mode shape and modal coordinate. As shown in Fig. 3, the piezoelectric patch is directly connected to the electrical resistance and the variable inductance. The variable inductance value is controlled with PWM as in Fig. 1 with two switches.

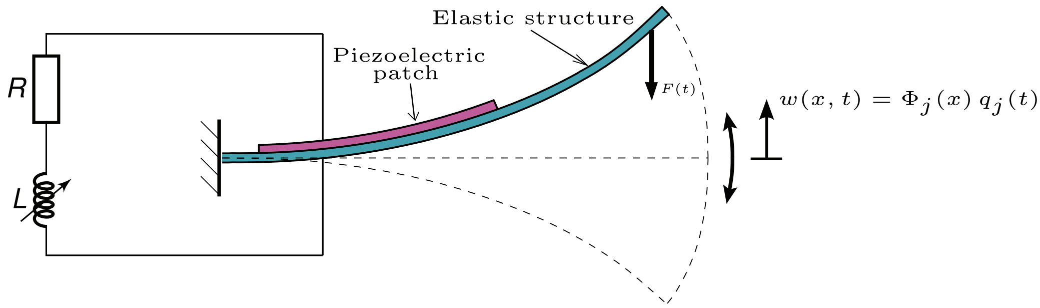

Figure 3: Vibrating elastic structure with a piezoelectric shunt composed of a tunable inductance with a resistance in series.

The state-space method used in the previous section yields to the following average electromechanical dynamic system:

$$\begin{cases} \ddot{q}_j + 2\zeta_j \omega_j \dot{q}_j + \hat{\omega}_j^2 q_j = \dfrac{F_j(t)}{m_j} + \dfrac{\chi_j}{m_j C_P} Q_C \qquad \forall j \in \{1, ..., N\} \; , \\ \ddot{Q}_C + \dfrac{\beta R + R_L}{L} \dot{Q}_C + \dfrac{\beta^2}{L C_P} Q_C = \dfrac{\beta^2}{L C_P} \displaystyle\sum_{j=1}^{N} \chi_j \, q_j \; , \end{cases} \tag{9}$$

where ζ_j, ω_j and m_j are the j-th modal damping ratio, pulsation (for the shunt in short-circuit) and modal mass of the structure, respectively. Accordingly to [11], we introduce the j-th piezoelectric coupling coefficient χ_j, the equivalent capacitance of the piezoelectric patch C_P and the electrical charge at the patch terminals Q_C. We also introduce the open-circuit natural pulsation of the j-th mode:

$$\hat{\omega}_j^2 = \omega_j^2 + \chi_j^2 / (m_j C_P) \; . \tag{10}$$

3.2 Effect of the duty cycle on the mechanical resonance

Applying the Fourier transforms on the governing Eq. (9) in the frequency domain [12] and normalizing the modal forcing by the modal shape (such as $F_j = F$), for the modes $j \in \{1, ..., N\}$, it yields to

$$\begin{pmatrix} Z_1 & \cdots & 0 & -\chi_1/C_P \\ \vdots & \ddots & \vdots & \vdots \\ 0 & \cdots & Z_N & -\chi_N/C_P \\ \bar{\omega}_e^2\,\chi_1 & \cdots & \bar{\omega}_e^2\,\chi_N & -Z_e \end{pmatrix} \begin{pmatrix} \breve{q}_1 \\ \vdots \\ \breve{q}_N \\ \breve{Q}_C \end{pmatrix} = \begin{pmatrix} \breve{F} \\ \vdots \\ \breve{F} \\ 0 \end{pmatrix} , \tag{11}$$

where, as previously, $\breve{\circ}(\Omega)$ denotes the Fourier transform of $\circ(t)$, the equivalent electrical pulsation $\bar{\omega}_e$ and the equivalent electrical damping $\bar{\zeta}_e$ are defined in Eq. 6. Moreover, we introduce the modal impedance $Z_j\,\forall j \in \{1, ..., N\}$ and the electrical impedance of the system Z_e as

$$Z_j = m_j\left(\hat{\omega}_j^2 - \Omega^2 + 2j\zeta_j\omega_j\Omega\right) , \qquad Z_e = \bar{\omega}_e^2 - \Omega^2 + 2j\bar{\zeta}_e\bar{\omega}_e\Omega \, . \tag{12}$$

Solving the linear system of Eq. (11) leads to the generalized mechanical mobility of the tunable resonant piezoelectric shunt coupled to an elastic structure for all $j \in \{1, ..., N\}$:

$$H_j(\Omega) = \frac{j\,\Omega\,\breve{q}_j}{\breve{F}} = \frac{j\,\Omega\left(C_P\,Z_e \prod\limits_{\substack{n=1\\n\neq j}}^{N} Z_n - \beta\,\bar{\omega}_e^2 \sum\limits_{\substack{n=1\\n\neq j}}^{N}\left[\chi_n\left(\chi_n - \chi_j\right) \prod\limits_{\substack{m=1\\m\neq\{j,n\}}}^{N} Z_m\right]\right)}{C_P\,Z_e \prod\limits_{n=1}^{N} Z_n - \beta\,\bar{\omega}_e^2 \sum\limits_{n=1}^{N}\left[\chi_n^2 \prod\limits_{\substack{m=1\\m\neq n}}^{N} Z_m\right]} \, . \tag{13}$$

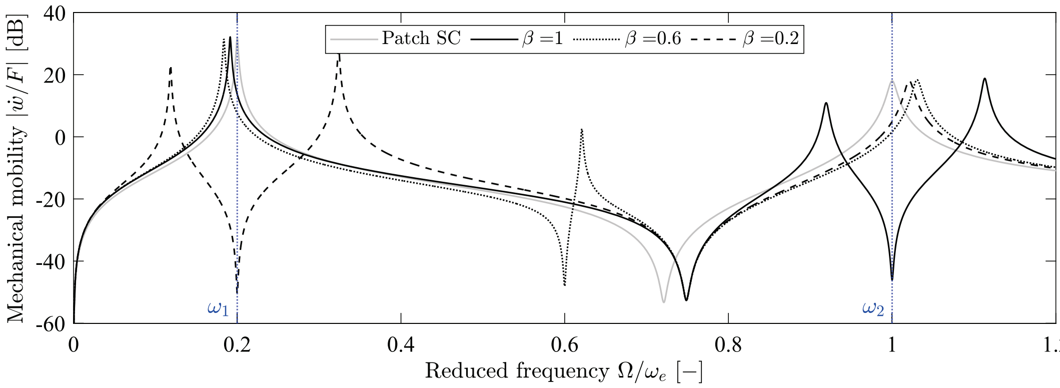

Figure 4: Modulus of the theoretical mechanical mobility of the elctromechanical system with the tunable inductance introduced in Fig. 3, about two modes of an arbitrary structure, $f_1 = 100\,$Hz and $f_2 = 500\,$Hz, and for three values of the duty-cycle β; Electromechanical parameters of the structure have been arbitrary set to $\zeta_1 = \zeta_2 = 0.005$, $m_1 = m_2 = 4\,$g, $\chi_1 = \chi_2 = 8\,$mN.V^{-1}, $C_P = 40\,$nF, $L = 2.44\,$H, $R = 5\,\Omega$ and $R_L = 1\,\Omega$.

Direct interpretation of key properties from the transfer function in Eq. 13 poses analytic challenges. To address this, Fig. 4 illustrates a case study analyzing two mechanical modes of a generic structural configuration. The duty-cycle value is set to different values with two of them adjusted to align the antiresonance with the natural frequency of the structure (with the piezoelectric shunt in short-circuit configuration). Once again, one can observe the antiresonance position in frequency linearly depending of the duty-cycle value. The operating range of the antiresonance variation is also validated for a large band of the duty-cycle domain. Note that the usable duty-cycle domain is independent of the initial value of the inductance and the tunable shunt is expected to work regardless the electrical parameters values.

4 EXPERIMENTAL VALIDATION

4.1 Practical chopper design

In practice, to obtain switches functional in the four quadrants of the voltage/current plan, diodes and MOSFET are combined as in the scheme of Fig. 5 where zones **A** and **B** refers to the switches in Fig. 3. Voltages at the MOSFET source and gate are controlled by the driver which delivers two isolated control signals from the Digital Signal Processor (DSP). A simplified representation of the connections between the DSP, the driver and the MOSFET is given in Fig. 5.

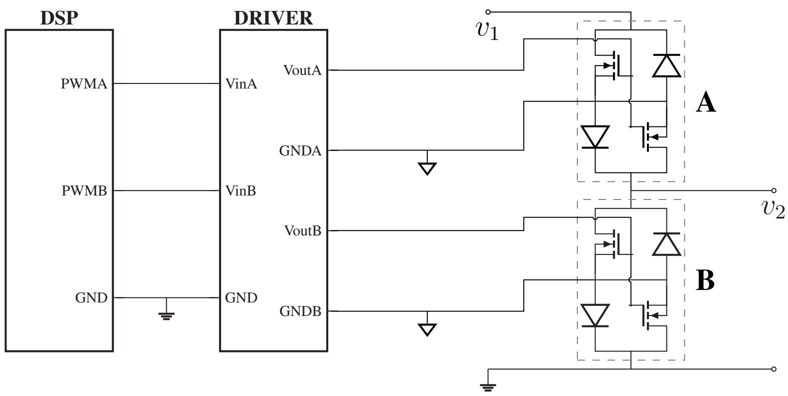

Figure 5: Practical 4-quadrants switches composed of two diodes and two MOSFET each; MOSFET are controlled by the driver with isolated control signals from ports PWMA and PWMB, the driver itself is managed by the Digital Signal Processor (DSP).

To prevent the chopper being in short-circuit during the transition state of the switches, the DSP also provide a dead-time of period T_m such as, in practice, the tunable shunt is monitored by the effective duty-cycle $\beta_\mathrm{eff} = \beta - T_\mathrm{m}/T_\mathrm{PWM}$ [10]. Here, the dead-time period is set such as $T_\mathrm{m}/T_\mathrm{PWM} = 0.004$.

4.2 Experimental setup

Prior to coupling the tunable shunt to an elastic structure, the core concept is experimentally validated using a simplified series RLC circuit (capacitor C and inductance L). The theoretical configuration of Fig. 1 is replicated experimentally, with the resistance R set to match the capacitor's internal resistance. A frequency-swept chirp signal, generated by a power amplifier driven by an m+p VibPilot controller, excites the circuit. Voltage measurements across the capacitor (V_C) and the RC branch (V_{in}) are acquired and processed in real time via the m+p VibPilot, as depicted in the experimental setup of Fig. 6(b). This preliminary step isolates the electrical resonance dynamics, ensuring unambiguous characterization before introducing mechanical coupling effects in subsequent structural tests.

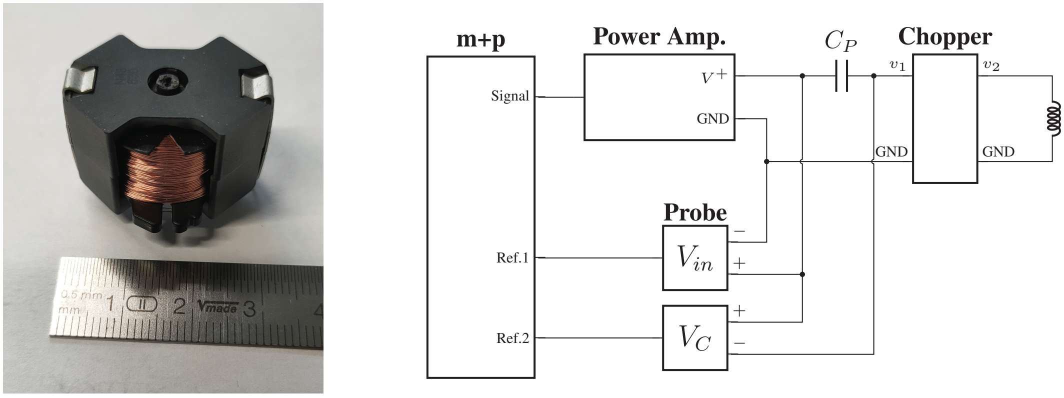

Figure 6: (a) Inductor made with a ferrite core for the experimental validation; (b) Scheme of the tunable LC circuit supplied by the power amplifier and with probes measuring the input voltage V_{in} and the voltage across the capacitor V_C.

The inductance is made of a coil of copper wire and a ferrite core as shown in Fig. 6(a). Commonly used for power applications, this kind of manufactured inductance allows reaching a value of $L = 1.06\,\text{H}$ and for an internal resistance of $R_L = 66\,\Omega$ (measured at $100\,\text{Hz}$). The electrical capacitor is chosen so that it has a low internal resistance and the electrical frequency f_e of the LC circuit is close to the firsts natural frequencies of the hydrofoil studied in the HYDRAVIB project ($\sim$ $100\,\text{to}\,1000\,\text{Hz}$). Then a capacitor of value $C_P = 660.2\,\text{nF}$ with an internal resistance $R_C = 3.33\,\Omega$ (measured at $100\,\text{Hz}$) is connected to the circuit. Regarding the expected frequency range of the electrical resonances, the switching frequency is set to $f_{\text{PWM}} = 2\,\text{kHz}$ which satisfies the 10:1 ratio requirement between the PWM frequency and the circuit's resonant frequency.

4.3 Assessment of the tuning performances

Thanks to the voltage signals measured across the capacitor and the RLC circuit, the electrical frequency response function (FRF) of V_c/V_{in} is drawn for different values of duty-cycle as seen in Fig. 7. First of all, it is shown that the electrical resonance frequency of the RLC circuit is accurately modified in comparison to the theoretical results. Moreover, as expected from the theory, the resonance magnitude decrease with the duty-cycle even if experimental results show a greater magnitude reduction when the PWM is activated ($\beta \neq 1$).

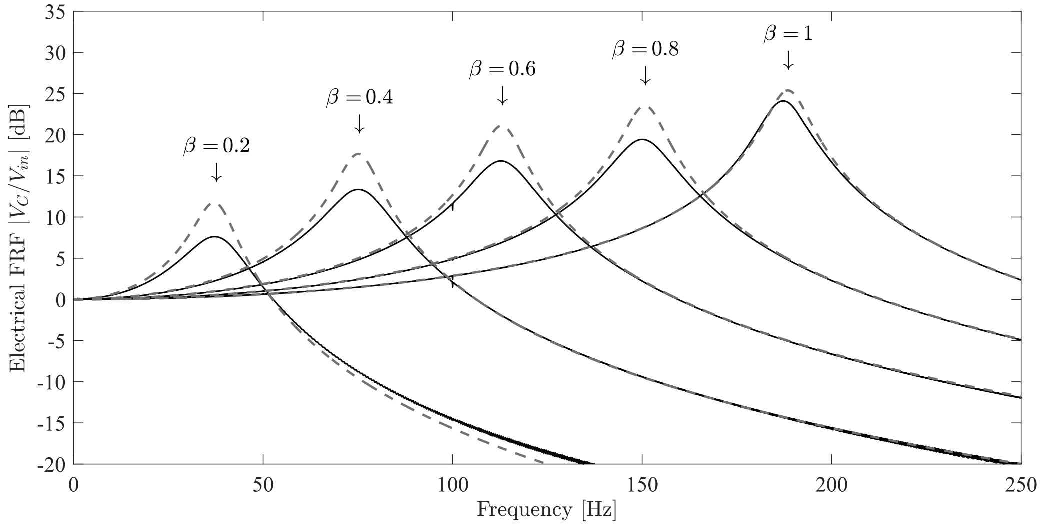

Figure 7: Modulus of the experimental electrical FRF V_c/V_{in}, represented in solid lines (—) of the tunable RLC circuit with $L = 1.06\,\text{H}$, $R_L = 66\,\Omega$, $C_P = 660.2\,\text{nF}$, $R = 3.33\,\Omega$ and for different values of β; Experimental data are compared to theoretical results, represented in dashed lines (- - -).

Experimental observations suggest the presence of a measurable parasitic resistance associated with the chopper circuit. While this phenomenon could theoretically originate from the switching components, its magnitude appears inconsistent with the low on-state resistance of the semiconductor devices, an apparent contradiction requiring further investigation. Systematic characterization of individual circuit elements will be necessary to isolate the underlying mechanism in future work.

5 CONCLUSIONS

Theoretical analyses presented in this work validate the tunable resonant shunt concept for both standalone RLC circuits and electromechanical coupled systems. The duty cycle β demonstrates precise control over the effective inductance, enabling targeted adjustment of the electrical resonance frequency (or antiresonance in coupled systems). Experimental validation on a simplified RLC circuit corroborates the theoretical framework, though measured responses exhibit unexpected over-damping. While preliminary evidence suggests switching losses in the chopper circuit as a plausible contributor, the exact source of this parasitic dissipation requires systematic characterization in future studies. Yet, even with a proper working tunable shunt, the theory suggests an increasing equivalent resistance while the duty-cycle decrease (refer to Eqs. (6) and (9)) and performance of the shunt may suffer when the duty-cycle β is set under 0.5 (risk of ending up with an over-resistive resonant shunt).

Future efforts will focus on two priorities: (1) implementing the tunable shunt on a piezoelectr coupled elastic structure to assess its vibration suppression capabilities under dynamic loading, and (2) experimental validation on a hydrofoil subjected to hydrodynamic flow to evaluate robustness in real-world marine environments. Concurrently, a detailed investigation into the origins of parasitic resistance (e.g., high-frequency eddy currents, PCB track impedance, or transient switching effects) will be conducted to resolve the observed damping discrepancy.

ACKNOWLEDGMENTS

The authors would like to express sincere gratitude to the *Agence de l'Innovation de Défense* (AID) and the *Agence Nationale de la Recherche* (ANR) for the support of the project HYDRAVIB (ANR-22-ASTR-0012).

REFERENCES

[1] M. Paidoussis, S. Price, and E. de Langre, *Fluid-Structure Interactions: Cross-Flow-Induced Instabilities*. Cambridge University Press, 2011.

[2] L. Pernod, B. Lossouarn, J. Astolfi, and J. Deü, "Vibration damping of marine lifting surfaces with resonant piezoelectric shunts," *Journal of Sound and Vibration*, vol. 496, p. 115921, 2021.

[3] Y. Watine, B. Lossouarn, C. Gabillet, J. A. Astolfi, and J. Deü, "Mitigation of hydrofoil torsional flow induced vibrations by resonant piezoelectric shunt," *Ocean Engineering*, vol. 313, p. 119598, 2024.

[4] O. Thomas, J. Ducarne, and J. Deü, "Performance of piezoelectric shunts for vibration reduction," *Smart Materials and Structures*, vol. 21, no. 1, p. 015008, 2012.

[5] J. F. Toftekær and J. Høgsberg, "Multi-mode piezoelectric shunt damping with residual mode correction by evaluation of modal charge and voltage," *Journal of Intelligent Material Systems and Structures*, vol. 31, no. 4, pp. 570–586, 2020.

[6] D. Niederberger, S. Behrens, A. Fleming, S. Moheimani, and M. Morari, "Adaptive electromagnetic shunt damping," *IEEE/ASME Transactions on Mechatronics*, vol. 11, no. 1, pp. 103–108, 2006.

[7] A. McDaid and B. Mace, "A self-tuning electromagnetic vibration absorber with adaptive shunt electronics," *Smart Materials and Structures*, vol. 22, no. 10, p. 105013, sep 2013.

[8] D. Niederberger, M. Morari, and S. Pietrzko, "Adaptive resonant shunted piezoelectric devices for vibration suppression," *Proc SPIE*, vol. 5056, 08 2003.

[9] Z. Shami, C. Giraud-Audine, and O. Thomas, "A nonlinear tunable piezoelectric resonant shunt using a bilinear component: theory and experiment," *Nonlinear Dynamics*, vol. 111, no. 8, pp. 7105–7136, 04 2023.

[10] M. Auleley, C. Giraud-Audine, H. Mahé, and O. Thomas, "Tunable electromagnetic resonant shunt using pulse-width modulation," *Journal of Sound and Vibration*, vol. 500, p. 116018, 2021.

[11] O. Thomas, J. F. Deü, and J. Ducarne, "Vibrations of an elastic structure with shunted piezoelectric patches: efficient finite element formulation and electromechanical coupling coefficients," *International Journal for Numerical Methods in Engineering*, vol. 80, no. 2, pp. 235–268, 2009.

[12] C. Close, D. Frederick, and J. Newell, *Modeling and Analysis of Dynamic Systems*. Wiley, 2001.